Capillary trapping of buoyant particles within regions of emergent vegetation

Citation: Peruzzo, P., A. Defina, and H. Nepf (2012), Capillary trapping of buoyant particles within regions of emergent vegetation, Water Resour. Res., 48, W07512, doi:10.1029/2012WR011944.

As Published: http://dx.doi.org/ 10.1029/2012WR011944

Publisher: American Geophysical Union (AGU)

Persistent URL: http://hdl.handle.net/1721.1/72492

Version: Final published version: final published article, as it appeared in a journal, conference proceedings, or other formally published context

Capillary trapping of buoyant particles within regions of emergent vegetation

Paolo Peruzzo,[1] Andrea Defina,[1] and Heidi Nepf[2]

Received 1 February 2012; revised 1 June 2012; accepted 6 June 2012; published 14 July 2012.

[1] The seeds of many aquatic plants are buoyant and thus transported at the water surface, where they are subject to surface tension that may enhance their retention within emergent vegetation. Specifically, seeds may be trapped by surface tension (i.e., by the Cheerios effect) at the surface-piercing interface of the vegetation. In this work we develop a physical model that predicts this mechanism of seed trapping, advancing the model proposed by Defina and Peruzzo (2010) that describes the propagation of floating particles through emergent vegetation. The emergent vegetation is simulated as an array of cylinders, randomly arranged, with the mean gap between cylinders far greater than the particle size, which prevents the trapping of particles between pairs of cylinders, referred to as net trapping. Laboratory experiments are used to guide and validate the model. The model also has good agreement with experimental data available in the literature for real seeds and more complex plant morphology.

Citation: Peruzzo, P., A. Defina, and H. Nepf (2012), Capillary trapping of buoyant particles within regions of emergent vegetation, *Water Resour. Res.*, *48*, W07512, doi:10.1029/2012WR011944.

1. Introduction

[2] Seed dispersal can play an important role in structuring aquatic habitat. The seeds of many aquatic plants are buoyant, which enhances their dispersal by keeping the seeds afloat for longer advection times [e.g., *Nilsson and Danvind*, 1997; *Van den Broek et al.*, 2005; *Nilsson et al.*, 2010]. The fate of these seeds within a region of vegetation is mainly controlled by the flow velocity and by the efficiency of a variety of seed-plant interaction mechanisms that trap the seeds [*Chambert and James*, 2009; *Defina and Peruzzo*, 2010]. The main mechanisms responsible for temporary or permanent trapping of particles are (1) inertial impaction [*Palmer et al.*, 2004], which occurs when a particle deviates from a streamline because of its inertia and collides with a stem; (2) wake trapping, which occurs when a particle enters the unsteady recirculation zone behind a stem [e.g., *White and Nepf*, 2003]; (3) trapping due to surface tension, i.e., the Cheerios effect, in which floating particles are attracted toward stems by the rising meniscus [e.g., *Vella and Mahadeven*, 2005]; and (4) net trapping, which occurs where leaves and/or stems overlap enough to form a netlike structure that intercepts the floating particle [*Defina and Peruzzo*, 2010]. When the mean gap between leaves or stems is comparable to the particle size, then net trapping is the most efficient trapping mechanism [*Defina and Peruzzo*, 2010, 2012]. Alternatively, when the mean gap between plant elements is large compared to the particle size, and flow velocity is moderately slow, then the Cheerios effect is the main, if not the only, mechanism impacting seed propagation, capture and diffusion [*Chambert and James*, 2009]. The present study considers the latter flow condition and develops a physically based model to predict the impact of surface tension (Cheerios effect) on the fate of floating particles within a region of emergent vegetation.

2. Model and Experimental Methods

[3] The emergent vegetation is simulated as an array of randomly arranged cylinders, each with diameter d. The array density is described by the cylinders per unit bed area, n. The cylinder spacing is assumed to be far greater than the particle size, which eliminates net trapping, i.e., the trapping of particles between a pair of cylinders. In this case the capture of floating particles by the cylinders is dominated by inertial impaction [*Palmer et al.*, 2004] and by the attraction due to the surface tension (i.e., the Cheerios effect).

2.1. Model

[4] As a particle advects through the array of cylinders, it passes, on average, one cylinder within each longitudinal distance, $\Delta s = (nd)^{-1}$, as shown in the work of *White and Nepf* [2003]. As each cylinder is passed, the particle has some probability of colliding with it, P_i, so that on average a particle will interact (collide) with a cylinder once per distance

$$\Delta s_i = \frac{\Delta s}{P_i} = \frac{1}{ndP_i}. \quad (1)$$

[1]Dipartimento di Ingegneria Civile, Edile e Ambientale (DICEA), Università di Padova, Padova, Italy.
[2]Department of Civil and Environmental Engineering, Massachusetts Institute of Technology, Cambridge, Massachusetts, USA.

Corresponding author: P. Peruzzo, Dipartimento di Ingegneria Civile, Edile e Ambientale (DICEA), Università di Padova, via Loredan 20, I-35131 Padova, Italy. (paolo.peruzzo@unipd.it)

0043-1397/12/2012WR011944

[5] Except for the extreme cases (i.e., for high cylinder density or very low flow velocity) we expect that the probability P_i does not depend on n. Preliminary experiments, discussed in section 3, confirm this.

[6] Observations have shown that particles may collide (interact) with several cylinders, before being captured by, i.e., permanently attaching to, a specific cylinder [*Defina and Peruzzo*, 2010]. Based on this, we separately define the process of interaction (collision followed by release) and the process of capture (permanent trapping). Below, the subscripts "i" and "c" will be used to denote parameters associated with interaction and capture, respectively.

[7] Following *Defina and Peruzzo* [2010], we define the probability $P(X > L)$ that a particle travels a distance X greater than L before being captured, as

$$P(X > L) = (1 - P_c)^{N_i}, \tag{2}$$

where P_c is the capture probability (i.e., the probability that a particle, which interacts with a cylinder, is permanently captured), and N_i is the number of interactions between a particle and the cylinders within the distance L, which we approximate as $N_i = L/\Delta s_i$. We can rewrite equation (2) as

$$P(X > L) = e^{L/\lambda}, \tag{3}$$

in which

$$\lambda = -\frac{\Delta s_i}{\ln(1 - P_c)} = -\frac{1}{ndP_i \ln(1 - P_c)} \tag{4}$$

is the mean distance traveled by a particle before it is permanently captured.

[8] In order to estimate P_i, and thus Δs_i, we consider the trajectory of individual particles as they pass an individual cylinder (Figure 1). For example, to describe inertial impaction, previous authors assumed that the particle trajectory was set by the fluid drag and particle inertia. A set of trajectories associated with these assumptions is shown in Figure 1a. The length-scale b is the distance between the outermost trajectories that lead to collision. Geometrically, $P_i = b/d$ (Figure 1). Models to predict b, and thus P_i, for inertial impaction are described in *Shimeta and Jumars* [1991] and *Palmer et al.* [2004].

[9] However, in this paper we focus on floating particles at low-flow velocity, for which the acceleration caused by surface tension (i.e., by the Cheerios effect) may be important drawing particles toward the cylinder from distances greater than d. An example of trajectories for surface particles influenced by surface tension is shown in the Figure 1b. Because it is possible for $b > d$, the probability of collision P_i can be greater than one. While this sounds contradictory, it is physically sound. It characterizes the fact that the influence of surface tension can generate more frequent cylinder collisions than would be predicted from the mean spacing, i.e., $\Delta s_i < \Delta s$. In section 2.2 we develop a model to predict b, and thus P_i, for floating particles influenced by surface tension.

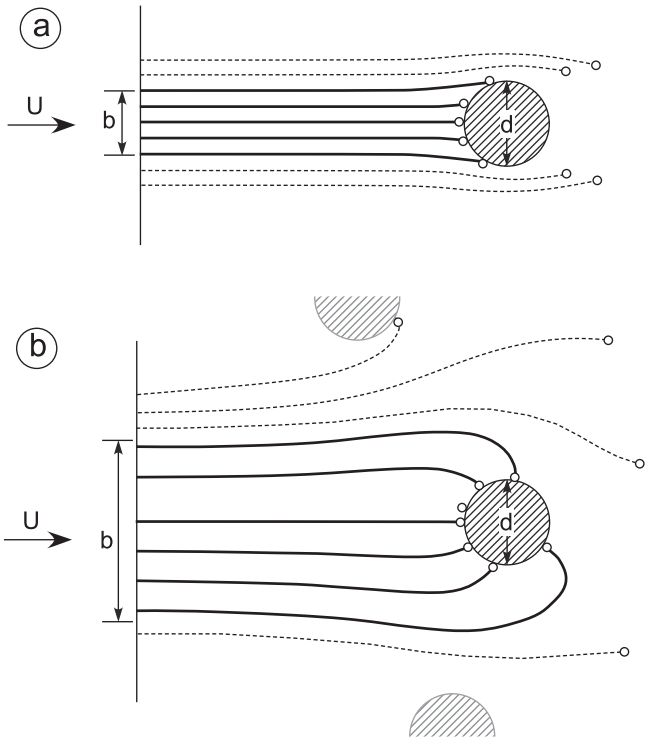

Figure 1. Definition sketch for the probability of particle collision (interaction) with a cylinder of diameter d. Solid lines indicate particle trajectories that lead to collision. The outermost trajectories that lead to collision are separated by distance b. The collision probability is $P_i = b/d$. (a) Inertial impaction occurs when the forces of drag and inertia dominate the particle trajectory approaching the cylinder. (b) For floating particles, the Cheerios effect adds to inertia and drag in controlling the particle trajectory, thus affecting the size of b.

2.2. Theoretical Prediction of P_i for Floating Particles Under the Influence of Surface Tension

[10] The Cheerios effect is influenced by the relative importance of inertial forces and surface tension. However, these two forces act on the particle in different directions, so that P_i cannot be parameterized simply by the ratio of the force magnitudes. Instead, we use a kinematic approach for defining P_i. For this description x and z are the streamwise and transverse coordinate directions, respectively (Figure 2). We define a rectangular area of influence, centered at the cylinder, whose edge in the x direction is the

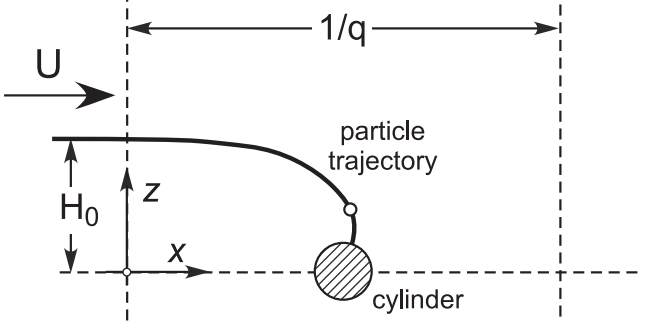

Figure 2. A particle trajectory influenced by surface tension which leads to collision with the cylinder. H_0 represents the maximum distance from the cylinder from which a particle can be drawn to collide with the cylinder by the action of surface tension. $H_0 = b/2$, with b defined in Figure 1.

capillary length, $1/q$, which is the characteristic length scale of the meniscus. In the z direction the edge has an infinite length. We assume that a particle crossing this area is attracted toward the cylinder through the Cheerios effect. If we assume that the particles move, on average, at the velocity U/β_q in the streamwise direction, with U the bulk flow velocity and β_q a correction factor, then, on average, a particle will spend time $T_q = \beta_q/(qU)$, within the zone of influence. T_q is also the time available for the Cheerios effect to draw a particle to the cylinder, before it leaves the influence of the cylinder. From this time-scale we can estimate the maximum distance from the cylinder, H_0, from which a particle can be drawn to collide with the cylinder by the action of surface tension (Figure 2).

[11] This maximum distance corresponds to $b/2$ of Figure 1, i.e., $b = 2H_0$ and

$$P_i = 2H_0/d. \tag{5}$$

[12] The distance H_0 is computed, as a first approximation, by assuming that only the capillary force acts on both the particle and the cylinder. The particle is assumed to be spherical. The capillary force, F_c, is given by [*Dushkin et al.*, 1996]

$$F_c = -\frac{\pi}{2} d_p d\sigma \sin(\alpha_p + \psi_p) \sin(\psi_p) \sin(\psi_c) K_1(qz). \tag{6}$$

[13] In (6) d_p is the particle diameter, α_p is the particle-water contact angle, ψ_p and ψ_c are the meniscus slope angles at the particle and cylinder contact line, respectively (defined in Appendix A), $\sigma = 0.073$ N m^{-1} is the surface tension, $q^{-1} = 0.0027$ m is the capillary length and $K_1(qz)$ is the modified Bessel function of the first kind, with z the transverse distance of the particle from the cylinder.

[14] The following differential equation governs the particle position, z,

$$\frac{d^2(qz)}{dt^2} = cK_1(qz), \tag{7}$$

with

$$c = \frac{3d\sigma q^2}{\rho_p d_p^2} \sin(\alpha_p + \psi_p) \sin(\psi_p) \sin(\psi_c), \tag{8}$$

and ρ_p the particle density. We assume that the particle starts from rest at position $z = H_0$, i.e., boundary conditions

$$t = 0 \begin{cases} z = H_0 \\ dz/dt = 0 \end{cases}. \tag{9}$$

[15] We approximate the Bessel function in equation (7) as $K_1(qz) \approx 1/(qz)^3$ for $qz < 5$, and find the solution as

$$qz = \sqrt{(qH_0)^2 - c(qH_0)^{-2} t^2}. \tag{10}$$

[16] The maximum distance, H_0, will be that associated with the maximum time available for lateral transport driven by surface tension, that is T_q. For simplicity, we assume that the particle collides with the cylinder at $z = 0$, i.e., neglecting the radius of both the cylinder and the particle (Figure 2). The impact of this assumption on the time-scale for the particle to reach the stem is absorbed into the scale constant within T_q, i.e., β_q. Then, setting $z = 0$ and $t = T_q$, we solve (10) for H_0

$$H_0^2 = \beta_q \frac{\sqrt{c}}{Uq^3}. \tag{11}$$

[17] Using (5), (8), and (11) we find

$$P_i = \frac{2H_0}{d} = \frac{2\sqrt{\beta_q}}{dq\sqrt{U}} \left[\frac{3d\sigma}{\rho_p d_p^2}\right]^{1/4} [\sin(\alpha_p + \psi_p) \sin(\psi_p) \sin(\psi_c)]^{1/4}. \tag{12}$$

[18] Since $We = \rho d U^2/\sigma$ is the Weber number, equation (12) can be rewritten as

$$P_i = \frac{\beta\sqrt{d/d_p}}{dqWe^{1/4}} \left(\frac{\rho}{\rho_p}\right)^{1/4} [\sin(\alpha_p + \psi_p) \sin(\psi_p) \sin(\psi_c)]^{1/4}, \tag{13}$$

where $\beta = 3^{1/4} 2\sqrt{\beta_q}$ and ρ is the water density. Experiments described in section 3 suggest $\beta = 2.46$, such that $\beta_q = 0.87$, which is close to unity, as expected.

2.3. Capture Probability P_c

[19] After a particle collides with a cylinder, it may become permanently attached, or it may be pulled away from the cylinder by the action of fluid drag. The probability of remaining permanently attached, P_c, depends on the ratio between the capillary force acting when the particle is stuck to the cylinder and the drag force due to the local mean flow, to turbulence and to vortex shedding. We assume that this drag force F_d, is proportional to the bulk velocity, U

$$F_d = k_d C_D \rho A_p U^2, \tag{14}$$

where k_d is a scale factor, A_p is the projected area of the submerged part of the particle and C_D is the particle drag coefficient.

[20] When the ratio of capillary force (6) to drag force (14) is large, the particle remains attached to the cylinder, i.e., $P_c = 1.0$. We define E_{cr} as the critical value of this force ratio above which the probability of capture becomes unity, i.e.,

$$E_{cr} = \frac{F_c}{F_d}\Big|_{P_c=1} = -\frac{\pi}{2} \frac{d_p d\sigma q}{k_d C_D \rho A_p U_e^2} \sin(\alpha_p + \psi_p) \sin(\psi_p) \sin(\psi_c) K_1\left(q\frac{d_p + d}{2}\right), \tag{15}$$

in which we define U_e as the escape velocity, i.e., the velocity above which particles may escape from the cylinder. We introduce the shape factor, k_p, which depends on the

particle draft (see Appendix A), such that $A_p = k_p d_p^2$, then rearrange (15) to describe the escape velocity, to

$$U_e^2 = \beta_e \frac{d}{d_p} \frac{\sigma q/\rho}{k_p C_D} \sin(\alpha_p + \psi_p) \sin(\psi_p) \sin(\psi_c) K_1 \left(q \frac{d_p + d}{2} \right), \tag{16}$$

with

$$\beta_e = \frac{\pi}{2 E_{cr} k_d}, \tag{17}$$

which we will use as a calibration parameter. Experimental investigations described and discussed in section 3 suggest $\beta_e = 1.26$.

[21] The escape velocity U_e is the scale velocity of the problem. When $U < U_e$ the capillary force is greater than the drag force no matter the position (with respect to the mean flow) at which the particle is stuck to the cylinder, therefore the probability of permanent capture is $P_c = 1$. When $U > U_e$, drag forces may locally and temporarily exceed the attraction force due to capillarity, and the particle may escape from the cylinder. Increasing of the ratio U/U_e reduces the probability P_c.

[22] The measurements, discussed below, suggest that the probability of capture P_c decays exponentially with U/U_e, specifically

$$P_c = \begin{cases} 1 & U/U_e \le 1 \\ e^{1-U/U_e} & U/U_e > 1 \end{cases}. \tag{18}$$

[23] From the models developed above we can now predict the following from the particle characteristics (d_p, ρ_p), the contact angles (α_p, α_c), the cylinder diameter (d), the stem density (n), and the bulk flow velocity (U): (i) the mean spacing between two interactions Δs_i from equations (1) and (13), (ii) the escape velocity U_e from equation (16), the capture probability P_c from equation (18), (iii) the mean distance a particle travels before it is permanently captured, from equation (4), and (iv) the path length distribution $P(X > L)$ from equation (3). In section 3 we use experimental observations to evaluate the two model parameters, $\beta = 2.46$ and $\beta_e = 1.26$.

2.4. Experiments

[24] To cover a wider range of flow conditions, two flumes are used in this investigation. The small flume has a channel width of 40 cm and length of 2.8 m, the large flume has a width of 120 cm and length of 13 m. In both flumes the water is recirculated by a pump that maintains steady flow. In both flumes the bottom is horizontal and the water depth is adjusted by a downstream weir. In the small flume the bulk flow velocity U is measured with an ADV (U is averaged over 33 points per cross section), while in the large flume U is estimated through a calibrated relationship between the pump frequency and the flowrate. The bulk velocity was varied between 0.7 and 5 cm s^{-1}. Seven of the velocity experiments were carried out in the small flume ($U = 0.007 - 0.032$ m s^{-1}), while higher velocity experiments ($U = 0.04$ and $U = 0.05$ m s^{-1}) were carried out in the large flume. In both flumes, a random array of cylinders was constructed on three boards to create a total test section length of 1.80 m. The array filled the flume width. We constructed six different arrays, with $n = 299$ m^{-2} to 1780 m^{-2}. The cylinders used in the experiments are wooden dowels with a diameter d of 6.0 mm, fitted into holes drilled into the boards.

[25] The model floating particles were cut from wood cylinders to have equal diameter and height of 3 mm (Figure 3). The relative density $\rho_r = \rho_p/\rho$ was $\approx$0.7. These are the same as particle C used by *Defina and Peruzzo* [2012].

[26] In the experiments, we release one particle at a time just upstream of the test section and at random positions in the transverse direction. For each experiment we released 200 particles. We observed the particle trajectory and measured the distance traveled by each particle, before it was permanently captured by a cylinder. We assumed a

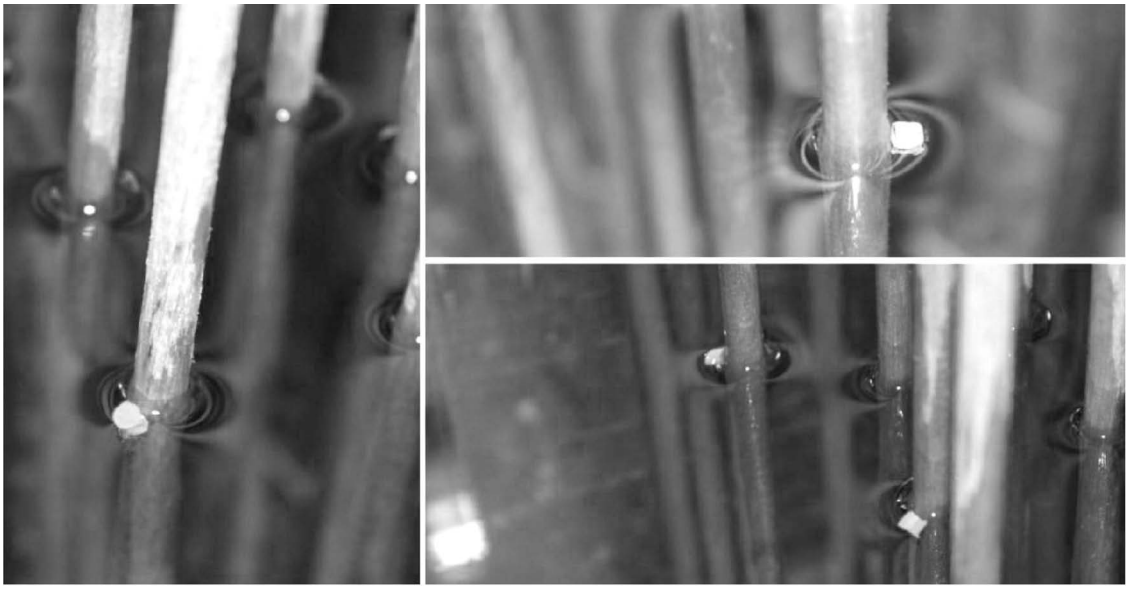

Figure 3. Snapshots of particles trapped against the cylinders through the Cheerios effect.

particle was permanently captured if it stayed stuck to one cylinder for more than 10 min, a time interval that was more than 1 order of magnitude longer than the mean time a particle took to travel the whole test section.

3. Results and Discussion

[27] We first consider the impact of cylinder density, n, while holding the bulk velocity constant ($U = 2.5$ cm s^{-1}). In all cases the exponential distribution given by (3) could be fit to experimental data with $R^2 > 0.95$. From this fit we extracted the mean path length, λ, for each stem density. From our theory, we expected that λ would have a dependence on the stem spacing, $\Delta s = (nd)^{-1}$ (see equation (4)). This relationship is observed in the measured λ (Figure 4). Since we use a single value of cylinder diameter, d, these graphs are plotted with n^{-1} alone. The data indicate a constant relationship between λ and n^{-1}, specifically $\lambda = 230/n$ for the present data (Figure 4, black circles). Since n is a constant, from (1) and (3) together, we can infer that the product $P_i \ln(1 - P_c)$ is also a constant. Consistent with the derivation above, we expect that the probability P_c is only a function of the flow near an individual cylinder, and that it does not depend on cylinder density, n. Then, P_i must also be independent of n.

[28] Further experiments were carried out with the aim of investigating how the model parameters change with the bulk flow velocity, U. The distance traveled by 200 particles is measured for $n = 968$ m^{-2} and seven different flow velocities (Table 1). In each case, the probability distribution of distances traveled by a particle before permanent capture followed an exponential law with $R^2 > 0.95$, except for the data with $U = 0.040$ m s^{-1} where, possibly because of the presence of a weak transverse seiche in the channel, the determination coefficient was lower ($R^2 = 0.90$), but still highly significant. Again, the exponential fit was used to determine the mean path length, λ, and to observe how this parameter varied with bulk flow velocity (see Table 1 and Figure 5). The dependence of λ on velocity comes through both P_i and P_c: notice that $P_i \sim U^{-1/2}$ (from equation (12)) and P_c is also inversely proportional to U (equation (18)), so that λ increases with increasing U (Figure 5). The behavior is consistent with physical reasoning: as velocity increases, the inertial forces become stronger relative to the capillary forces, leading to reduced interaction and capture by stems.

Table 1. Summary of Present Experimental Data and Model Parameters[a]

U (m s^{-1})	We (10^2)	Re	P_i	Δs_i (m)	λ (m)	P_c
0.007	0.403	42	2.32	0.074	0.021	0.971
0.009	0.666	54	2.05	0.084	0.025	0.965
0.017	2.380	102	1.49	0.116	0.086	0.739
0.020	3.290	120	1.37	0.125	0.110	0.680
0.025	5.140	150	1.23	0.140	0.234	0.451
0.028	6.440	168	1.16	0.148	0.353	0.343
0.032	8.420	192	1.09	0.159	0.642	0.219
0.040	13.200	240	0.97	0.177	1.357	0.122
0.050	20.500	300	0.87	0.198	3.549	0.054

[a]The observed travel distances for 200 particles are fit to (3) to find λ. P_i is predicted from (13). Δs_i is predicted from (1). The experimental estimates of P_c are based on (4), $P_c = 1 - \exp[-1/(nd\lambda P_i)]$, and P_i predicted from (13).

[29] Using the set of nine (U, λ) pairs, we calibrated the model parameters β and β_e. First, we used the following trial and error procedure to find β. We fixed a tentative value for β and used it to compute the probability of interaction, P_i, from equation (13), which in turn is used to find the mean spacing between interactions Δs_i from (1) and (13). Together with the observed λ, we find the capture probability P_c from equation (4). With nine pairs of (P_c, U), we find U_e by fitting equation (18). The value for β is then tuned to until we find the best fit to (18).

[30] Second, using the best-fit value for β, β_e is computed from (16). In this computation we used $d_p = 0.003$ m,

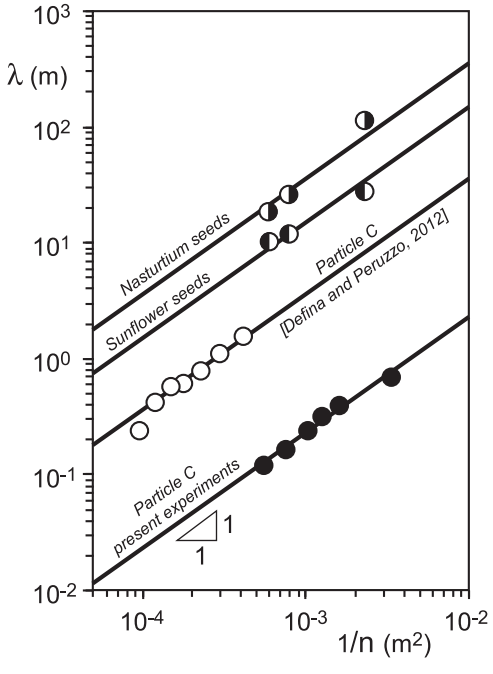

Figure 4. Mean path length as a function $1/n$. Present experimental results ($U = 0.025$ m s^{-1}, black circles aligned along the curve $\lambda = 230/n$); *Defina and Peruzzo* [2012] experimental results with particle C and $U = 0.033$ m s^{-1} (white circles, $\lambda = 3600/n$); and (half-full symbols) experimental data for *Nasturtium* ($\lambda = 3.5 \times 10^4/n$) and *Sunflower* seeds ($\lambda = 1.5 \times 10^4/n$) [*Chambert and James*, 2009].

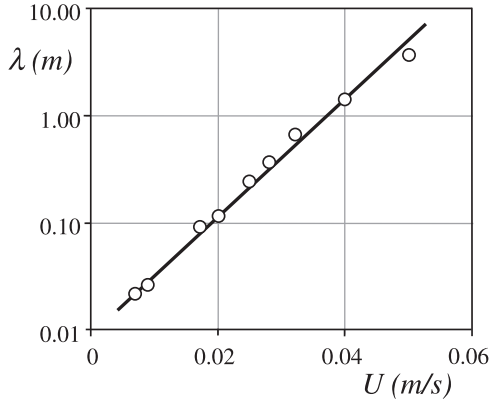

Figure 5. Mean path length as a function flow velocity in log linear scale (present experiments).

$\rho_r = 0.7$, and the measured contact angles $\alpha_p = 60°$ and $\alpha_c = 55°$ for the particle and the cylinder, respectively. We computed $\psi_p = 1.55$. (see Appendix A) and $\psi_c = 90° - \alpha_c = 35°$. Through this procedure we find $U_e = 0.013$ m s^{-1}, $\beta = 2.46$ and $\beta_e = 1.26$.

[31] With these values, the interaction probability P_i, the mean spacing Δs_i, and the probability P_c are computed as given in Table 1. The theoretical model for P_c (equation (18)) is shown as a solid line in Figure 6. The values of P_c estimated for individual cases are shown by symbols. The experimental estimates of P_c are based on (4), $P_c = 1 - \exp[-1/(n\lambda dP_i)]$, using the measured value of λ, and P_i predicted from (13).

[32] We now use experimental results from previous studies, *Defina and Peruzzo* [2010, 2012] and by *Chambert and James* [2009], to validate the model. These studies consider particle sizes and stem diameters which are different from those in the present study.

[33] *Defina and Peruzzo*'s [2010, 2012] experiments were carried out in a 6 m long, 0.3 m wide tilting flume. The bed slope and a downstream weir were adjusted to achieve uniform flow conditions with a water depth of ≈0.1 m. The model plant canopy consisted of plastic plants inserted into a perforated Plexiglas board covering the middle 3 m length of the flume. The plants were arranged either randomly or in a staggered pattern. The plastic plants, which resemble *Spartina Maritima*, were 0.15 m high and composed of approximately 120 leaves per model plant. Here, we tentatively assume that each leaf piercing the free surface can be represented as a cylinder having a diameter of 2 mm, which corresponds to the larger dimension of the leaf, which has an elliptical cross-section. This leaf diameter is smaller than the particle diameter, d_p (see Figure 7). Three different particles were used in the experiments to mimic different buoyant seeds: particle *A* was a wood particle with diameter of ≈2.5 mm and a relative density of 0.95, particle *B* (see Figure 7) was a smooth spherical berry with a mean diameter of 3.7 mm and a relative density of 0.83, and particle *C* was the same particle used in the present experiments.

[34] For particle *C*, *Defina and Peruzzo* [2012] showed that the mean path length λ varied inversely with the number of plants per unit area n_p, i.e., $n_p\lambda = \text{const}$. Since each plant had the same number of leaves, the mean path length also varies inversely with the number of leaves (i.e., cylinders) per unit area, as shown in Figure 4.

[35] From equations (1) and (4) we have $n\lambda = -1/[dP_i \ln(1 - P_c)]$. The constant value $n\lambda$ differs, in the different experiments by orders of magnitude (see Figure 4). For example, compare the present study ($\lambda = 230/n$) with the *Defina and Peruzzo* [2012] experiments ($\lambda = 3600/n$), which use the same particle, but different stem diameter and velocity. The difference in λ is explained in part by the difference in velocity. Using the data in Table 1, we can see that an increase in velocity from 0.025 m s^{-1} to 0.033 m s^{-1} increases λ by a factor of 2.7. The remaining difference (an additional factor of about 5.7) can be attributed to the difference in stem diameter which affects P_i and P_c through U_e. On comparing the present study with the *Chambert* [2006] experiments, which use the same cylinder diameter, the differences can be ascribed to the different particle diameter, which affects both P_i and P_c and, mainly, to the different flow velocity: in the *Chambert* [2006] experiments velocity is 6.4 times the present velocity; as such both P_i and P_c reduces dramatically.

[36] In the study from the work of *Defina and Peruzzo* [2010], individual leaves were, in some places, spaced closely enough to create net trapping, so that the probability of capture, P_c, measured in those studies reflects both the net trapping and the trapping associated with the

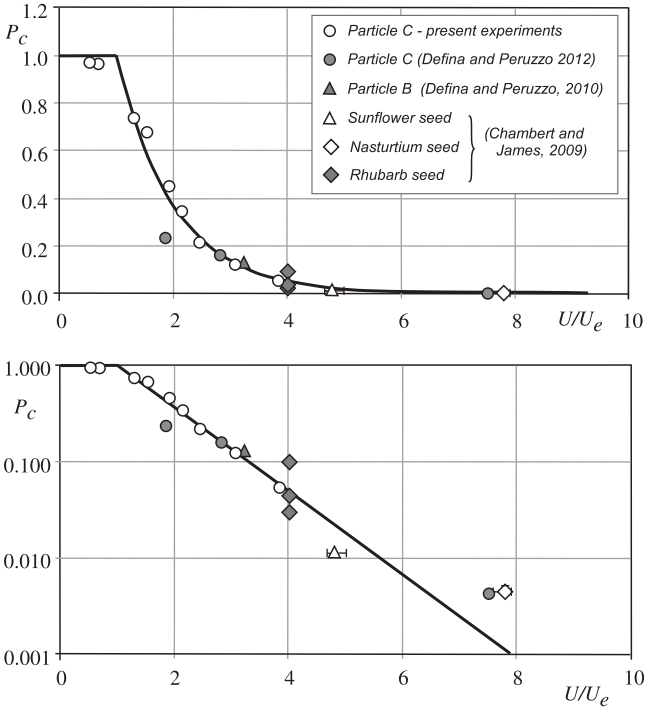

Figure 6. Comparison between theoretical and experimental probability of capture as it varies with U/U_e. The capture probability is plotted both in (top) natural scale and (bottom) logarithmic scale.

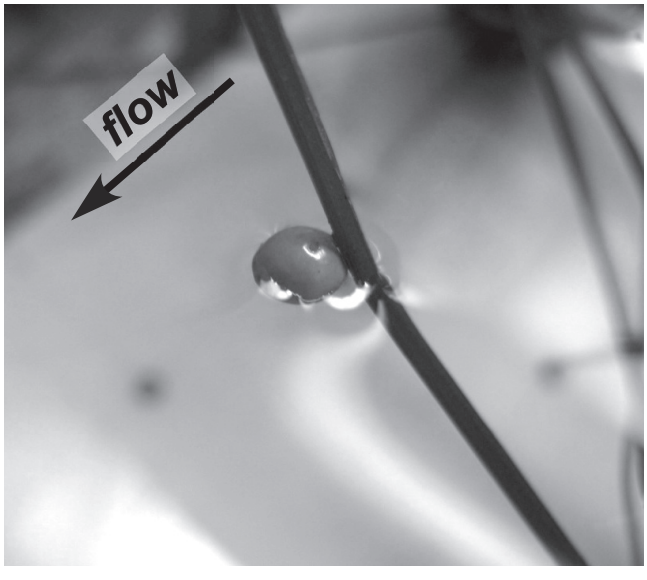

Figure 7. Particle *B* attached to a leaf through the Cheerios effect.

Cheerios effect. The theory presented here only accounts for the Cheerios effect, and so we must isolate that mechanism from the data reported by *Defina and Peruzzo* [2010]. We assume that the probability of capture due solely to the Cheerios effect is given by the measured total probability of capture (which includes the net trapping mechanism) times the measured percentage of captures due to the Cheerios effect, which is reported in the work of *Defina and Peruzzo* [2010]. Moreover, for the plastic leaves we measured a contact angle $\alpha_c \approx 30^\circ$ so that $\psi_c = 90^\circ - \alpha_c \approx 60^\circ$. Experimental data as well as the results of the computations are given in Table 2.

[37] The values of P_c and U/U_e reported in Table 2 are included in Figure 6. The *Defina and Peruzzo* [2010] data points are consistent with the model curve (solid line) developed for an array of cylinders. This agreement is encouraging, especially given the rather different experimental conditions and possible uncertainties, e.g., *Spartina* leaves are not cylinders, some of the net-trapping captures may actually have been through the Cheerios effect, i.e., net trapping may mask some of the captures through the Cheerios effect. These experimental results suggest that the relationships proposed in the present paper to estimate the model parameters when the Cheerios effect is the dominant capture mechanism can be extended, with due care, to real plants. In this connection, an allometric study to establish the equivalence between real plant morphologies and the diameter and density of a group of cylinders could be of use.

[38] *Chambert and James* [2009] experiments were conducted in a 20 m long and 0.38 m wide flume. The model vegetation comprised an array of cylinders with a diameter of 0.006 m, arranged across the full width of the flume in staggered pattern. The total array length was 1.88 m, and the array began 1 m downstream from the seed feeder. Three sets of experiments were carried out with the three different stem densities given in Table 3 and the same mean flow velocity, $U = 0.16$ m s^{-1}. Five types of natural, buoyant seeds were used for the experiments: *African Daisy*, *Nasturtium*, *Rhubarb*, *Sunflowers*, and *Marigold*. The flume was fed with 300 seeds during 4 min, and the flow was stopped after a total duration of 8 min. The number of seeds retained (i.e., permanently captured) was then counted visually (see Table 3).

[39] The mean path length given in Table 3 was calculated from (3), specifically

$$\lambda = \frac{1}{-\ln[P(X > L)]},$$

where we take $L = 1.88$ m, and $P(X > L)$ is the percentage of noncaptured seeds, i.e., $P(X > L) = 1 - N_c/300$. Please note that the estimation of λ is rather uncertain, because it uses data for a single value of L, rather than a large set of data (P, L) to fit $P(X > L)$, as in the present experiments.

[40] In addition, the experimental procedure adopted by *Chambert and James* [2009] is different from the present experiments. We follow the trajectory and fate of one particle at a time, whereas *Chambert and James* [2009] release all the 300 seeds in 4 min, allowing the seeds to accumulate within the array. As a result, when the number of captured seeds is large, seeds released near the end of the run find little or no room to interact with the cylinders, and may instead attach, to previously captured seeds (see, e.g., their Figure 14), forming clusters of seeds within the array. The clustering likely increases the probability of capture for seeds released later in the run, a behavior that is not included in the present model. As a consequence the mean path length λ of the lighter seeds (i.e., *African Daisy*, *Marigold*, and *Rhubarb*), which are more easily trapped and thus exhibited more clustering, does not follow $1/n$, as observed in the present study. However, the heavier seeds, *Nasturtium* and *Sunflower*, which did not form clusters, exhibit the relationship $\lambda \sim n^{-1}$ consistent with the model developed in this paper (Figure 4).

[41] We use data for *Nasturtium* and *Sunflowers* seeds to compute P_c as it varies with U/U_e. We assume a contact angle α_p in the range 15°–35° for *Sunflowers* seeds, whereas for *Nasturtium* seeds we measured a contact angle $\alpha_p = 17.5^\circ$. In both cases we assume, for the cylinder, a contact angle $\psi_c = 55^\circ$ (i.e., the same contact angle for the cylinders used in the present experiments). We then compute the meniscus slope angle at the particle contact line ψ_p, the escape velocity U_e and the interaction probability P_i (see Table 4).

[42] Combining equations (4) with (1) we have

$$\ln(1 - P_c) = -\frac{1}{P_i d n \lambda}.$$

[43] We use $d = 0.006$ m and the mean experimental value for $n\lambda$ ($n\lambda \approx 3.5 \times 10^4$ m^{-1} for *Nasturtium* seeds and $n\lambda \approx 1.5 \times 10^4$ m^{-1} for *Sunflowers* seeds, Figure 4) in the above equation to compute the probability of capture P_c (shown in Table 4). These values are also plotted in Figure 6, and they compare favorably with the theoretical curve. It is interesting to observe in Table 4 that the capture probability is not very sensitive to the contact angle α_p so that uncertainties in evaluating α_p have a minor impact on the estimation

Table 2. Summary of Experimental Conditions and the Results of Present Computations[a]

Particle	d_p (mm)	$\rho_{p/\rho}$	α_p (deg)	ψ_p (deg)	U (m s^{-1})	U_e (m s^{-1})	P_c
A	2.5	0.95	–	–	0.073	–	–
A	2.5	0.95	–	–	0.081	–	–
B	3.7	0.83	35	3.55	0.073	0.020	0.13
C	3.0	0.70	60	1.55	0.033	0.016	0.24
C	3.0	0.70	60	1.55	0.050	0.016	0.16
C	3.0	0.70	60	1.55	0.133	0.016	0.02

[a]Experimental conditions come from the work of *Defina and Peruzzo* [2010, 2012]. Data in italic is unpublished.

Table 3. Number of Captured Seeds N_c and Mean Path Length λ Between Brackets, for the Three Different Stem Densities n[a]

Seed Type	$n = 431$ (m^{-2})	$n = 1251$ (m^{-2})	$n = 1681$ (m^{-2})	CSF
Sunflower	20;(27.2)	44;(11.9)	51;(10.1)	0.43
African Daisy	194;(1.8)	204;(1.6)	215;(1.5)	0.19
Marigold	134;(3.2)	155;(2.6)	162;(2.4)	0.15
Rhubarb	137;(3.1)	141;(3.0)	149;(2.7)	0.54
Nasturtium	5;(111.9)	21;(25.9)	29;(25.9)	0.87

[a]The Corey Shape Factor (CSF), which measures the seed roundness, is also given as reported by *Chambert* [2006]. N_c is out of 300. λ is in meters and n is in m^{-2}.

Table 4. Summary of Seed Characteristics and Computed Model Parameters[a]

Seed Type	Average Diameter (mm)	Mass (g/seed)	$\rho_{p/}\rho$	$nd\lambda$	α_p (deg)	ψ_p (deg)	U_e (m s^{-1})	P_i	P_c
Sunflower	6.2	0.0576	0.46	77	15–35	21.0–29.5	0.035–0.032	1.11–1.15	0.011–0.012
Nasturtium	7.0	0.1320	0.73	227	12–19	18.8–23.5	0.021–0.022	0.98–1.00	0.004–0.005
Rhubarb	4.7	0.0169	0.32	8; 22; 28	38–46	14.7–16.9	≈0.039	1.19–1.21	0.099–0.100: ≈0.037; ≈0.030

[a]The average seed diameter is computed as the geometric average of the three axes reported in the work of *Chambert* [2006]: orthogonal long d_1, intermediate d_2 and short axes d_3. The seed density is computed as the ratio of seed mass [*Chambert*, 2006] to the volume of a sphere having the average diameter.

of P_c. For example, for the *Sunflowers* seeds a 40% change in α_p ($\alpha_p = 25^\circ \pm 10^\circ$) leads to only a minor (2.2%) change in P_c ($P_c = 0.01135 \pm 0.00025$); for the *Rhubarb* seeds a 23% change in α_p ($\alpha_p = 15.5^\circ \pm 3.5^\circ$) leads to a 8.8% change in P_c ($P_c = 0.0048 \pm 0.0004$). Finally, we also computed the capture probability for *Rhubarb* seed, which, among the three lighter seeds, has the greatest roundness (CSF), and thus comes closest to fitting the assumptions of the theoretical equations used to predict meniscus slope angle ψ_p (see Appendix A). Since the product $n\lambda$ is not constant in this case, we computed three different values for P_c using the mean path lengths given in Table 3 for the three different cylinder densities. Results are plotted in Figure 6 and again a good agreement with the theory is found.

4. Conclusions

[44] In this work we improve upon the model developed by *Defina and Peruzzo* [2010] by reducing model complexity and by developing a physically based prediction for model parameters. We focused on the role of surface tension in capturing floating seeds within emergent vegetation. Two scaling parameters within the model were estimated using data from the present study of floating particles within an array of cylinders. Observations from *Defina and Peruzzo* [2010, 2012], which consider a different morphology of model plant, and from *Chambert and James* [2009], which considers real floating seeds, compare favorably with the model predictions, validating the model and confirming that it can be extended to other plant and seed morphologies. Indeed, the good agreement between model predictions and experimental results by *Defina and Peruzzo* [2012], with plants having a moderately complex geometry, suggests that the model can be used, with due care, with natural vegetation, provided that stem density is relatively small so that net trapping can be neglected, and that flow velocity is sufficiently slow so that the Cheerios effect is comparable to inertia.

Appendix A: Evaluation of the Meniscus Slope Angle ψ_p

[45] The meniscus slope angle at the particle contact line ψ_p is estimated by the dynamic analysis of vertical forces acting on a floating sphere (see Figure 8). For light particle ($\rho_p < \rho$) the equilibrium position is reached when the weight of the sphere and the surface tension in the vertical direction are balanced by the pressure force acting on the sphere

$$\frac{\pi d_p^3}{6}\rho_p g + 2\pi r_i \sigma \sin(\psi_p) = \pi h^2\left(\frac{d_p}{2} - \frac{h}{3}\right)\rho g - \rho g \Delta h \pi r_i^2. \quad \text{(A1)}$$

[46] Because of elementary geometric considerations the contact radius is

$$r_i = d_p \sin(\vartheta_p)/2 \quad \text{(A2)}$$

with $\vartheta_p = \alpha_p + \psi_p$ and α_p the contact angle of the particle. Equation (A1) can be rewritten as

$$\frac{\pi d_p^3}{6}\rho_p g + \pi\sigma \sin(\psi_p)\sin(\vartheta_p) = \pi h^2\left(\frac{d_p}{2} - \frac{h}{3}\right)\rho g. \quad \text{(A3)}$$

[47] The contact radius r_i can also be written as

$$r_i = \sqrt{\frac{d_p^2}{4} - \left(\frac{d_p}{2} - h\right)^2}. \quad \text{(A4)}$$

[48] From equations (A2) and (A4) the sphere immersion h can be expressed as a function of ϑ_p

$$h = \frac{d_p}{2}[1 + \sqrt{1 - \sin^2(\vartheta_p)}] = \frac{d_p}{2}[1 + \cos(\vartheta_p)]. \quad \text{(A5)}$$

[49] Replacing (A5) In (A3) and rearranging, the equilibrium position of the sphere is given by

$$\sin(\vartheta_p)\sin(\psi_p) + Bo\left[\frac{\rho_r}{6} - \frac{2 + 3\cos(\vartheta_p) - \cos^3(\vartheta_p)}{24} + \frac{\sin^2(\vartheta_p)\Delta h}{4 d_p}\right] = 0, \quad \text{(A6)}$$

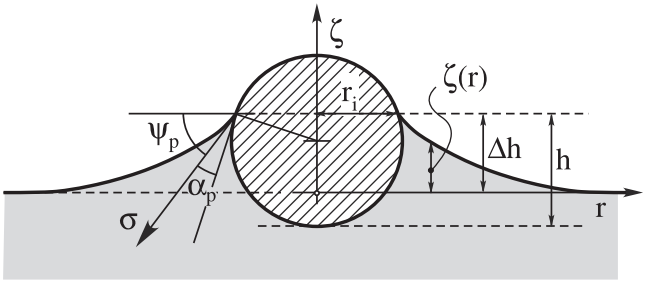

Figure 8. Forces acting on floating particle with density $\rho_p < \rho$; σ is the surface tension acting along the wetted perimeter.

where $\rho_r = \rho_p/\rho$ is the relative density of the sphere and $Bo = \rho g d_p^2/\sigma$ is the Bond number that represents the ratio between gravitational force and surface tension.

[50] According to *Kralchevsky and Nagayama* [2000] the shape of the meniscus wetting the sphere (see Figure 8) is given as

$$\zeta(r) = r_i \sin(\psi_p) K_0(rq), \tag{A7}$$

where $1/q$ is the capillary length and K_0 is the modified Bessel function of order 0.

[51] Replacing (A2) in equation (A7) we obtain the rise of the meniscus with respect to the undisturbed free surface

$$\Delta h = \frac{d_p}{2} \sin(\vartheta_p) \sin(\psi_p) K_0\left(\frac{d_p q}{2} \sin(\vartheta_p)\right). \tag{A8}$$

[52] By replacing (A8) in (A6) the equilibrium condition becomes

$$\sin(\vartheta_p)\sin(\psi_p) + Bo\left[\frac{\rho_r}{6} - \frac{2 + 3\cos(\vartheta_p) - \cos^3(\vartheta_p)}{24} + \right. \\ \left. + \frac{\sin^3(\vartheta_p)\sin(\psi_p) K_0\left(\frac{d_p q}{2}\sin(\vartheta_p)\right)}{8}\right] = 0 \tag{A9}$$

which can be used to compute the meniscus slope angle ψ_p.

[53] **Acknowledgment.** We gratefully acknowledge Chris James for his helpful comments. This research has been partially supported by the Fondazione Aldo Gini, Padova, Italy.

References

Chambert, S. (2006), Sorting of seeds by hydrochory, Master's thesis, Dep. of Civ. and Environ. Eng., Chalmers Univ. of Technol., Gothenburg, Sweden.

Chambert, S., and C. S. James (2009), Sorting of seeds by hydrochory, *River Res. Appl.*, *25*, 4861, doi:10.1002/rra.1093.

Defina, A., and P. Peruzzo (2010), Floating particle trapping and diffusion in vegetated open channel flow, *Water Resour. Res.*, *46*, W11525, doi:10.1029/2010WR009353.

Defina, A., and P. Peruzzo (2012), Diffusion of floating particles in flow through emergent vegetation: Further experimental investigation, *Water Resour. Res.*, *48*, W03501, doi:10.1029/2011WR011147.

Dushkin, C. D., P. A. Kralchevsky, V. N. Paunov, H. Yoshimura, and K. Nagayama (1996), Torsion Balance for measurement of capillary immersion forces, *Langmuir*, *12*, 582–592.

Kralchevsky, P. A., and K. Nagayama (2000), Capillary interactions between particles bound to interfaces, liquid films and biomembranes, *Adv. Colloid Interface Sci.*, *85*, 145–192.

Nilsson, C., and M. Danvind (1997), Seed floating ability and distribution of alpine plants along a northern Swedish river, *J. Veg. Sci.*, *8*, 271–276.

Nilsson, C., R. L. Brown, R. Jansson, and D. M. Merritt (2010), The role of hydrochory in structuring riparian and wetland vegetation, *Biol. Rev.*, *85*, 837–858.

Palmer, M. R., H. M. Nepf, and T. J. R. Pettersson (2004), Observations of particle capture on a cylindrical collector: Implications for particle accumulation and removal in aquatic systems, *Limnol. Oceanogr.*, *49*(1), 76–85.

Shimeta, J., and P. A. Jumars (1991), Physical mechanisms and rates of particle capture by suspension feeders, *Oceanogr. Mar. Biol. Annu. Rev*, *29*, 191–257.

Van den Broek, T., R. Van Diggelen, and R. Bobbink (2005), Variation in seed buoyancy of species in wetland ecosystems with different flooding dynamics, *J. Veg. Sci.*, *16*(5), 579–586.

Vella, D., and L. Mahadeven (2005), The "Cheerios effect," *Am. J. Phys.*, *73*(9), 817–825.

White, B. L., and H. M. Nepf (2003), Scalar transport in random cylinder arrays at moderate Reynolds number, *J. Fluid Mech.*, *487*, 43–79.